Article
Vol. 25, No. 1, p. 71–81, February 2021
https://doi.org/10.1007/s12303-020-0040-9
pISSN 1226-4806 eISSN 1598-7477
Geosciences Journal GJ

Assessment of seismic vulnerability using the horizontal-to-vertical spectral ratio (HVSR) method in Haenam, Korea

Su Young Kang[1], Kwang-Hee Kim[2]*, and Byungmin Kim[3]

[1]Institute of Geologic Hazard & Industrial Resources, Pusan National University, Busan 46241, Republic of Korea
[2]Department of Geological Science, Pusan National University, Busan 46241, Republic of Korea
[3]School of Urban and Environmental Engineering, Ulsan National Institute of Science and Technology, Ulsan 44919, Republic of Korea

ABSTRACT: The town of Haenam in southwest Korea lies partially on reclaimed coastal land and experienced an unprecedented earthquake swarm during April and May 2020. Construction of a new town in the area means that there is demand to evaluate the seismic hazard caused by site-specific amplification of seismic ground motions by artificial unconsolidated cover. We used a microtremor horizontal-to-vertical spectral ratio (HVSR) method to identify resonance frequencies, image depths to bedrock, and assess seismic ground vulnerability across the epicentral area of the recent earthquake swarm. Microtremor measurements were taken at 144 sites across an 18.5 km × 12.5 km study area. The HVSR analysis shows resonance frequencies as low as 1.1 Hz. Using mean shear-wave velocities obtained by Multi-Channel Analyses of Surface Waves (MASW), we find that resonance frequencies correspond to depths to bedrock of between 3 m and 56 m. There are clear relationships between the distribution of resonance frequencies, depths to bedrock, surface geology, and areas of development in recent land reclamation projects. Higher resonance frequencies characterize areas of thin sedimentary cover or hard rock sites, while relatively low resonance frequencies characterize reclaimed land or greater depths to bedrock. We quantify the seismic hazard potential across the study area using the seismic vulnerability of ground index (K_g), and observe a clear association between zones of high K_g and areas of reclaimed land. This study demonstrates the value of the HVSR technique in characterizing the subsurface and assessing seismic vulnerability in areas of reclaimed land, where it can be used as a viable and low-cost alternative to large-scale active seismic refraction or MASW measurements. The results can also be used to inform and guide urban planning projects.

Key words: Haenam earthquake swarm, horizontal-to-vertical spectral ratio method, resonance frequency, ground vulnerability index, urbanization

Manuscript received August 14, 2020; Manuscript accepted September 7, 2020

1. INTRODUCTION

On 3 May 2020, an M_L (local magnitude) 3.1 earthquake occurred in Haenam in southwestern Korea (Figs. 1 and 2a). The earthquake, which had a maximum Modified Mercalli Intensity (MMI) of III, was the first felt by residents in the area since modern seismic observations began in Korea in 1978. The earthquake was part of a sequence that occurred between 26 April and 10 May 2020. The spatiotemporal distribution of events indicated that this sequence was highly swarm-like, in contrast to tectonic mainshock-aftershock or foreshock-mainshock-aftershock sequences (Fig. 2b). Although the series of earthquakes did not cause any significant damage, residents in the area and local and federal authorities expressed serious concerns about earthquake hazards and risks to nearby communities. Since swarm-like seismicity is unusual on the Korean Peninsula, and the epicentral area is not known to have experienced previous earthquake activity, the sequence generated significant attention in local and national media.

During the initial stages of the 2020 Haenam earthquake swarm, the Pusan National University Geophysics Laboratory (PNUGL) mobilized a temporary seismic network to monitor the earthquake sequence. The temporary network was set up on

*Corresponding author:
Kwang-Hee Kim
Department of Geological Science, Pusan National University, Busan 46241, Republic of Korea
Tel: +82-51-510-2250, Fax: +82-51-5187-6389,
E-mail: kwanghee@pusan.ac.kr

Electronic supplementary material
The online version of this article (https://doi.org/10.1007/s12303-020-0040-9) contains supplementary material, which is available to authorized users.

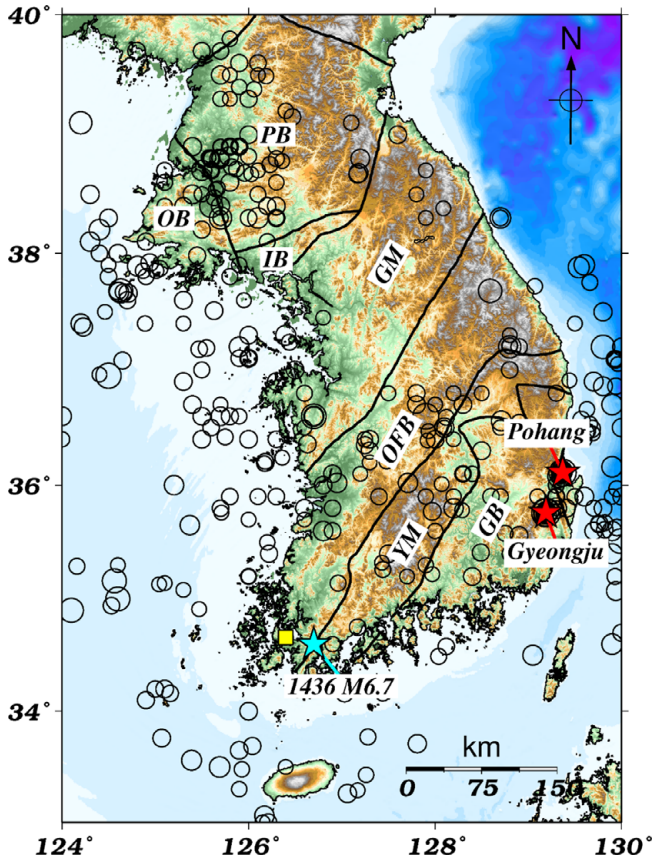

Fig. 1. Epicenter locations (black circles) of $M_L \geq 3$ earthquakes that have occurred in the Korean Peninsula since 1978, overlain on a topographic map of the region. The sizes of circles are scaled based on event magnitude. The epicenters of two recent, moderate-magnitude earthquakes in southeastern Korea are shown by red stars. The epicentral location of the highest-magnitude historic (1436) earthquake to have occurred in the region is marked by a cyan star. The location and extent of the study area is denoted by the yellow square. Major tectonic provinces are shown: PB = Pyungnam Basin, OB = Ongjin Basin, IB = Imjingang Belt, GM = Gyeonggi Massif, OFB = Okcheon Fold Belt, YM = Yeongnam Massif, GB = Gyeongsang Basin.

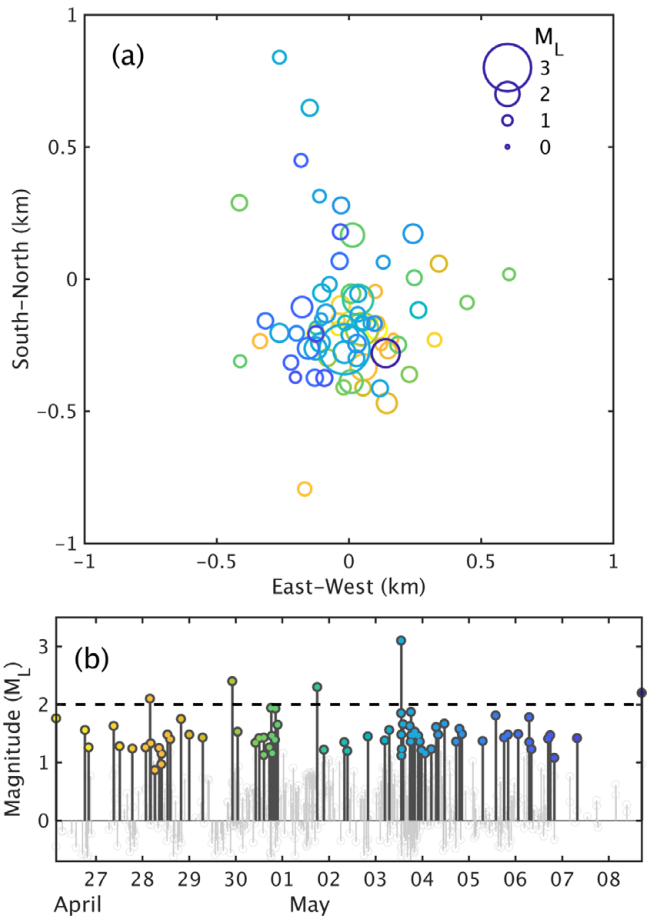

Fig. 2. Spatial and temporal distribution of the Haenam earthquake swarm sequence of April and May 2020. (a) Epicenter locations of earthquake swarm events in the study area (see yellow square in Fig. 1 for location). Sizes and colors of circles are scaled based on event magnitude and source time as outlines in figure part (b). The coordinates are given in kilometers east and north from a reference point at 126.4006°E and 34.6587°N. (b) Time-magnitude (M_L) distribution of events within the Haenam earthquake sequence. Earthquakes reported by the Korea Meteorological Administration are shown as colored circles. Gray lines with open circles indicate micro-earthquakes only identifiable by a detailed analysis of seismic waveforms.

1 May 2020 and consisted of eight three-component short-period seismic sensors, which were used to successfully record most of the swarm activity, including the largest earthquake (M_L 3.1) in the sequence (see Han et al., 2020) in this volume for details of PNUGL temporary seismic network at Haenam). Earthquake locations show that the epicentral area of swarm seismicity lies within a region undergoing substantial urban development associated with construction of the new (smart) city of SolaSeaDo (Jeollanamdo, 2020). Here, we investigate the seismic hazards associated with site amplification in the broader epicentral area of the 2020 Haenam earthquake swarm, including, but not limited to, the area of the SolaSeaDo city development. The results of our study are of particular importance because this region has not experienced significant earthquake activity for at least 42 years prior to the Haenam swarm, and therefore the seismic hazards and risks associated with the SolaSeaDo urban development have not been previously investigated.

Ground motions experienced at a site are the result of a combination of (1) earthquake source; (2) path effect (between source to the bedrock-sediment interface); (3) site effect (the sedimentary layer, e.g., bedrock-sediment interface to ground surface). Recent studies have shown that local site effects are a key influence on earthquake ground motions (Ishihara and Koga, 1981; Anderson et al., 1986; Seed et al., 1991; Holzer, 1995; Huang and Tseng, 2002). Indeed, in certain settings the vulnerability of an area to earthquakes depends more on site conditions than any other factor that influences ground shaking. It is now widely accepted that ground motions on sites containing soft soil are significantly stronger than those on nearby rock outcrops. A

striking example that illustrates this point is the 1985 M_S 8.1 Mexico earthquake. Despite the fact that the epicenter of this earthquake was located at a distance of ~400 km from Mexico City, the downtown area suffered severe damage during this event, resulting in more than 10,000 casualties and ~USD 6 billion of damage. Areas of severe damage generally coincided with areas covered by ancient lake sediments, while only minor damage was caused to a nearby town (located several kilometers from downtown Mexico City) situated on volcanic bedrock (Anderson et al., 1986; Reiter, 1991).

Estimation of the level of potentially damaging earthquake ground motion requires an evaluation of the site response, but this can be challenging where local seismic sources are scarce. In this study, we use the horizontal-to-vertical spectral ratio (HVSR) technique excited by the ambient noise of ground micro-motions (or microtremors). As the HVSR method requires only three-component noise measurements to calculate resonance frequencies, it is especially useful to constrain deep basin structures and estimate the earthquake site response in regions of low seismicity. We apply the HVSR technique to ambient noise data acquired during field surveys undertaken by PNUGL at 144 temporary sites across the wider epicentral area of the Haenam earthquake swarm (Fig. 3), which allows us to produce both resonance frequency and seismic vulnerability maps of the region. We also use Multi-Channel Analyses of Surface Waves (MASW) to constrain the shear-wave velocity of the shallow subsurface, and to estimate the depth to the bedrock at each site where ambient noise was measured.

The main objectives of this study are 1) to determine the fundamental frequency and peak amplitude of HVSR for each site, 2) to determine the depth to the high impedance contrast basement and the overall distribution of unconsolidated sediments, and 3) to estimate the potential ground-shaking hazards across the 2020 Haenam earthquake swarm epicentral area.

The southern Korean Peninsula has typically been regarded as a stable continental region in which the risk of seismic hazards is very low. Many papers published as recent as 2015 assert that seismic hazards and risks in Korea are negligible, which has strongly influenced public perception. However, two destructive earthquakes in Gyeongju in 2016 (M_L 5.8) and in Pohang in 2017 (M_L 5.4) – both located in southeastern Korea – have changed this viewpoint and resulted in a heightened awareness of seismic risk among local and central authorities, as well as the general public. Despite the fact that both of these damaging earthquakes occurred in southeastern Korea, we still do not have sufficient information to adequately address seismic hazards and risks in this region. This paper provides important preliminary results on earthquake hazards and risks associated with site effects in southwestern Korea, and promotes an open exchange of ideas and information regarding the 2020 Haenam earthquake.

2. GEOLOGICAL SETTING AND SEISMICITY

The Korean Peninsula is located on the margin of the Eurasian Plate, between the continental blocks of North and South China and the Japanese island arcs. The Peninsula consists of three

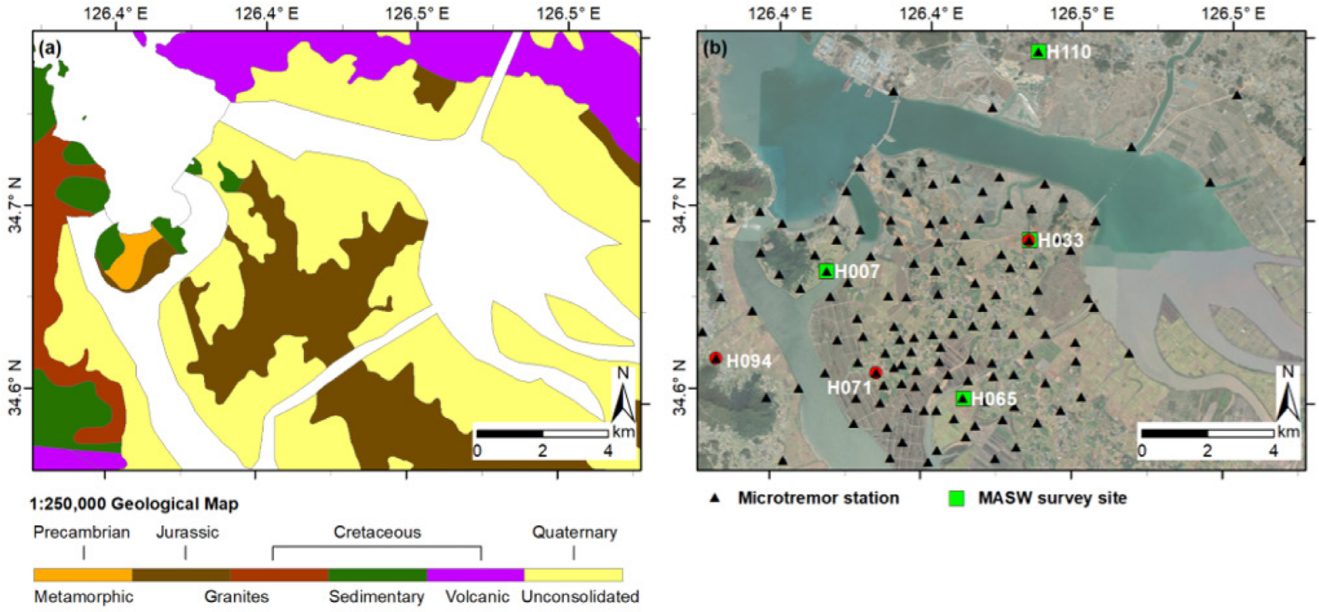

Fig. 3. Geological map and distribution of seismic stations. (a) Geological map of the study area (modified from KIGAM (2020)). Yellow areas (unconsolidated) are mainly areas of man-made materials associated with the large-scale land reclamation project that began in the late 1980s. (b) Locations of 144 seismic stations where ambient noise measurements were recorded for HVSR (black triangles) and 4 MASW survey sites for shear-wave velocity characterization (green squares). Locations of three HVSR examples in Figure 5 are shown by red circles. Note HN03 in Figure 5d (a hardrock site) is located outside the figure and is not shown.

https://doi.org/10.1007/s12303-020-0040-9

Precambrian basement massifs (the Nangrim, Gyeonggi, and Yeongnam massifs) separated by northeast-southwest striking fold belts. The 2020 Haenam earthquake swarm occurred in the southwestern Okcheon Fold Belt (OFB). The OFB separates the southern Korean Peninsula into the Gyeonggi massif in the northwest and the Yeongnam massif in the southeast (Fig. 1). Extensive faulting and fracturing occurred during a complex history of deformation in the OFB, mainly associated with brittle sinistral shearing in a retro-arc setting during early Cretaceous northward subduction of the Izanagi Plate (Chough et al., 2000). A prominent model for the tectonic evolution of the region (Yin and Nie, 1993) suggests that the Honam Shear Zone, located along the boundary between the OFB and the Yeongnam massif, represents the suture zone between the North China Block (Sino-Korea Craton) and the South China Block (Yangtze Craton). In this model, the Honam Shear Zone (Korea) and the Tanlu Fault (China) are lithospheric-scale transform faults associated with collision between the Sino-Korea and South China blocks. According to a teleseismic receiver function study by Chang and Baag (2007), the crustal thickness of the southern Korea Peninsula varies from 25.9 km to 32.5 km. The depth to the Moho near the 2020 Haenam earthquake swarm epicentral area is ~32 km.

The most recent geological map of the study area shows several large NNE-SSW striking faults, including the Gwangju Fault, and several smaller (unnamed) WNW-ESE striking faults (KIGAM, 2020). It is noteworthy that this area has been the focus of an extensive land reclamation project, which has dramatically changed the landscape and coastal morphology. A series of satellite images from 1984 to 2020 clearly captures changes in the shoreline and vegetation, with most of the previously intertidal regions becoming dry land. Additionally, construction on and around reclaimed land has occurred during urban development associated with the 33.84 km^2 SolaSeaDo city project, which was initiated in the mid-1990's (Jeollanamdo, 2020) (Fig. 4).

The area selected for study is 18.5 km × 12.5 km in size. Prior to urban development, the surface environment consisted primarily of Jurassic granites that were surrounded by intertidal regions. However, land reclamation since the late 1980's has significantly changed the nature of the surface environment. Details of the subsurface structure, including the depth to the major impedance contrast below intertidal zones and reclaimed land, remain poorly known. Two shallow high-resolution seismic reflection surveys carried out within intertidal areas on the western coast of Korea have revealed sharp subsurface discontinuities (Hong et al., 1999; Jou et al., 2008). Relatively shallow units in the intertidal zone are water-saturated and characterized by low seismic velocities and low densities. These units overlie bedrock with relatively high density and high seismic velocity. The large impedance contrast across this discontinuity makes the intertidal zone an ideal place to test the applicability of the HVSR technique for mapping the thickness of unconsolidated sediments. Both previous high-resolution seismic reflection surveys showed the major discontinuity at ~40 m depth. Based on these observations, we expect a relatively thin layer of unconsolidated sediment to overlie Jurassic granitic basement in our study area.

Historical earthquake data indicate that the wider Haenam region has experienced multiple felt earthquakes as large as MMI VIII-IX, including an M_L 6.7 event on 29 May 1436 (Lee

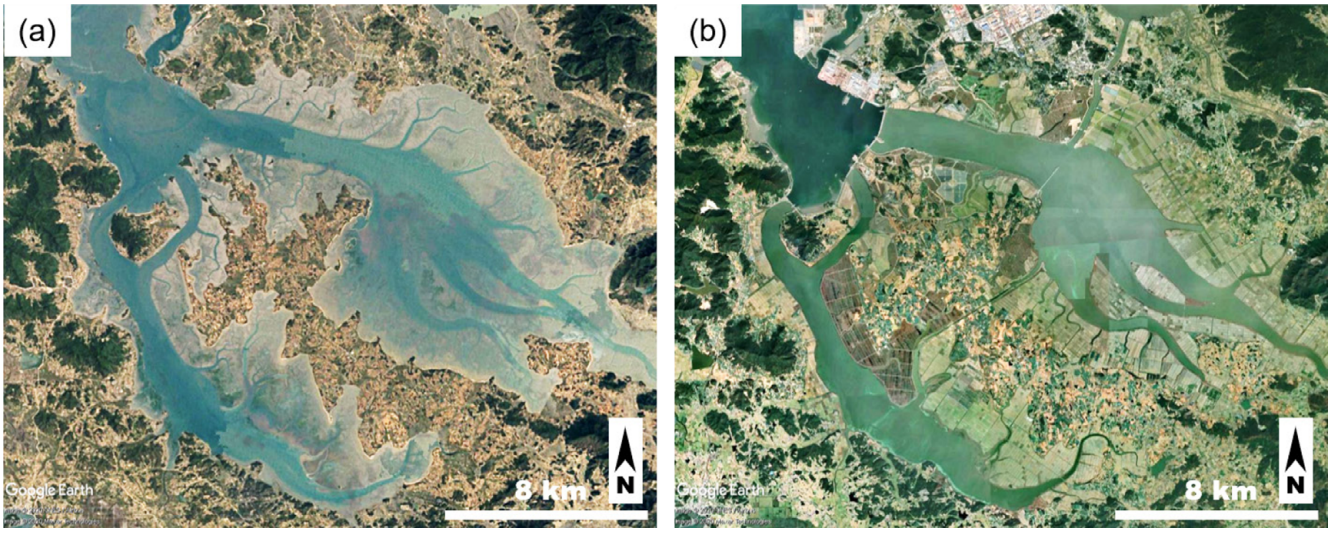

Fig. 4. Changes in shorelines and vegetation coverage within the study area between 1984 and 2020. (a) The satellite image taken in 1984 shows the area prior to the start of the large-scale reclamation project. (b) Current shorelines, vegetation, and urbanization are shown in the satellite image taken in 2020. Images are taken from Google Earth (2020).

and Yang, 2006) (Fig. 1). Details of previous seismicity in Haenam and swarm-type seismicity in Korea are discussed in a contribution by Kyung (2020) in this special issue. Despite multiple large events in historical earthquake records, seismic activity in the Haenam region was very low from 1978 (when seismic monitoring began in Korea) until the 2020 earthquake swarm. Abrupt seismicity started with a microearthquake (M_L 1.8) on 26 April 2020 and continued for two weeks (Fig. 2b). The largest earthquake in the sequence occurred on 3 May 2020. Event hypocenters from the sequence are highly clustered at ~20 km depth. Earthquake waveforms in the sequence are very similar, implying comparable locations and faulting mechanisms. The temporal distribution of event magnitudes is typical of swarm-type seismicity: a sequence of seismic events with no identifiable mainshock occurring in a local area within a relatively short period of time. Earthquake swarms have been recognized in different geological settings, and although swarm-type behavior is well understood in volcanic areas, it is relatively poorly understood in continental regions. Recent studies have attributed swarm-type seismicity at mid-crustal depths to the movement of meteoric or mantle-derived fluids through the brittle-ductile transition of large crustal faults (Becken et al., 2011; Dahm et al., 2013). However, the mechanisms and conditions driving occasional short-lived earthquake swarms in several locations (and at various depth ranges) throughout Korea are not well understood.

3. METHODS AND DATA

The horizontal-to-vertical spectral ratio (HVSR) method was proposed by Nakamura (1997, 2019). The method has been successfully applied to estimate the depth to an impedance contrast beneath a three-component seismic recording site. The HVSR method is a passive seismic method and therefore does not require an artificial seismic source. The method measures ambient noise using a three-component seismometer, and estimates the resonance frequency by the ratio of horizontal to vertical components of the Fourier amplitude spectra. Resonance frequencies are inversely proportional to the depths of high impedance contrasts, and can be interpreted to ascertain the thickness of unconsolidated sediments (Nakamura, 1989).

For stations located over simple structures, such as a single layer over a half-space, only one impedance contrast is expected, and HVSR curves present a single and clear fundamental resonance frequency and corresponding peak amplitude (Figs. 5a and c). Lower fundamental resonance frequencies correspond to thicker sedimentary layers. However, HVSR results for stations above more complex subsurface structures – consisting of two or more layers over a half-space – may show multiple peaks and resonance frequencies (Fig. 5b). The fundamental resonance frequency in these cases may be determined by taking into account additional information, such as local geological features and topography, and the resonance frequencies at adjacent sites (Nakamura, 1989; Bottelin et al., 2019). Lateral heterogeneity may also lead to multiple peaks. HVSR curves with no clear peak are also frequently observed and are indicative of very weak impedance contrasts (Fig. 5d). Consolidated sedimentary materials with high density and shear-wave velocity would result in comparable results.

Resonance frequencies obtained using the HVSR method are converted to thicknesses of sedimentary layers, which can then be interpreted in terms of the sedimentary basin structure or bedrock morphology. This is achieved via the simple relationship,

$$F_r = \frac{\overline{V}_s}{4Z}, \tag{1}$$

where F_r is the resonance frequency, Z is the thickness of the sedimentary layer, and $\overline{V}_s$ is the mean shear-wave velocity of the sedimentary layer above the bedrock (Lachet and Bard, 1994; Ibs-von Seht and Wohlenberg, 1999; Lee et al., 2017). In our study, we obtain a representative mean shear-wave velocity for shallow deposits using MASW surveys conducted at four sites throughout the study area. For each MASW survey, 24 geophones (with a natural frequency of 4.5 Hz) were installed at 1 m or 2 m spacings, depending upon site conditions. A sledgehammer was used as an active source, and passive ambient noise data were also collected for analysis. We utilized the ParkSEIS v3.0 program (Park, 2018) to automatically process the MASW data and conduct dispersion analysis using the phase-shift method (Park et al., 1999), which selects the phase velocity at the highest summed amplitude for each frequency. We then implemented the searching algorithm of Xia et al. (1999) to invert the dispersion curves and estimate the shear-wave velocity and the thickness of soil layers.

We use the HVSR method to characterize the potential site response and to quantitatively assess the seismic hazard and risk through calculation of the seismic vulnerability index (K_g) across the wider epicentral area of the 2020 Haenam earthquake swarm. A fundamental goal of earthquake engineering is to increase the durability of both the ground surface and built structures to a threshold seismic force. If areas or structures of high vulnerability are identified prior to damaging earthquakes, it is possible to reinforce them in advance. The damage caused by an earthquake depends on the intensity, frequency, and duration of the associated ground motions. It is well-known that stronger ground motions are expected to occur in thick, soft soil or unconsolidated deposits (Abd El-Aal, 2010; Liu et al., 2014). The characteristics of the ground surface can be identified by analyzing the resonance frequencies of HVSR of microtremor. The ground motions at a given site that occur in response to an earthquake are known to

https://doi.org/10.1007/s12303-020-0040-9

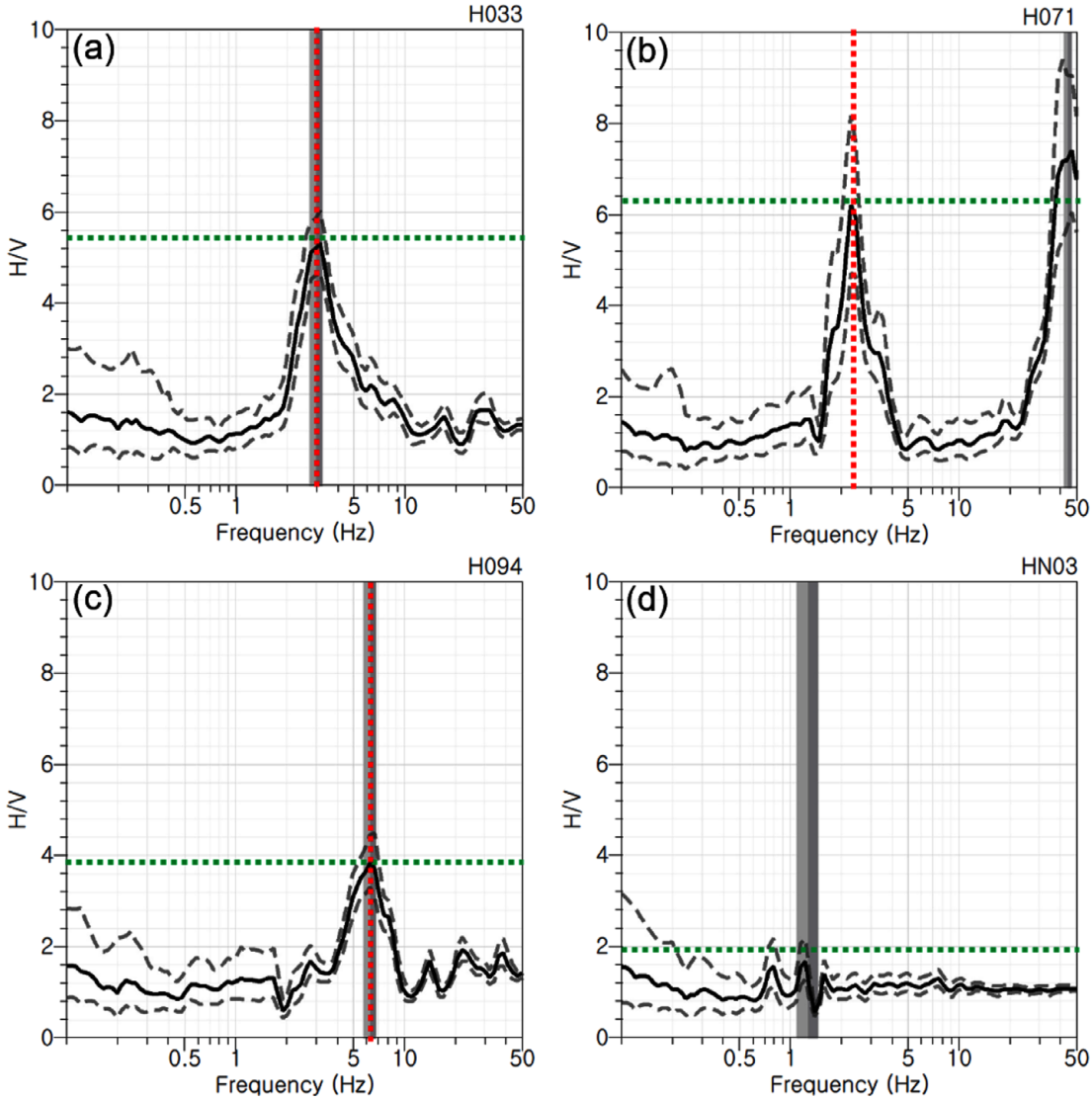

Fig. 5. Examples of typical HVSR curves (solid black lines) ± one standard deviation (dashed grey lines) obtained from selected stations (top-right of each panel). (a) HVSR curve with a single peak at a medium frequency. (b) HVSR curve with multiple peaks. (c) HVSR curve with a single peak at a higher frequency. (d) HVSR curve with no peaks. The shaded vertical lines and red dashed vertical lines in each panel represent the resonance frequencies determined by the processing software (GEOPSY) and by manual analysis, respectively. The green horizontal lines show the maximum amplitudes of the interpreted fundamental resonance frequencies.

be proportional to the dynamic strain caused by seismic vibrations, and may be expressed as a seismic vulnerability index (K_g) given by the relationship.

$$K_g = A^2/F_r\,. \tag{2}$$

Here, A is the amplification factor of horizontal to vertical motion, F_r is the fundamental resonance frequency, and K_g is considered to be an intrinsic index representing the vulnerability of the ground and structures to earthquake shaking (Nakamura, 1997; Liu et al., 2014). The value of K_g may be associated with large errors at sites where it is difficult to determine the absolute amplification factor. In the derivation of K_g, Nakamura (1997) assumed that the acceleration experienced by basement rocks in response to a seismic wave does not vary significantly over a local area. Thus, the effective shear strain recorded at the ground surface can be used as a relative measurement of a site's vulnerability, with respect to other sites in the same area (Hardesty et al., 2010). Seismic vulnerability index maps produced using HVSR are a powerful tool to identify hazardous areas prone to significant ground movement. HVSR has several advantages over alternative methods used to assess seismic vulnerability, including: low cost; non-invasive data collection; simple and flexible instrumentation requirements that enable rapid field data collection; rapid processing times; and intuitive and practical interpretation of data. Although we limited our

study of seismic vulnerability to shaking at ground levels, the method can be readily extended to include multi-story structures (Trunbull, 2009).

In order to estimate depths to impedance contrasts and to characterize earthquake site responses within the 2020 Haenam earthquake swarm area, HSVR microtremor measurements were conducted at 144 sites in the study area (Fig. 3b). At each site, ambient noise was recorded by three-component velocity-type seismometers for a period of at least 30 minutes, at a sampling rate of 250 Hz. Microtremor measurements were completed over a period of two weeks by two teams of experienced field technicians. As the study area was located away from any major population centers, anthropogenic noise in the seismic records was limited. Seismometers were also buried 0.3 m below the surface to reduce any contributions from surface noise and wind (Kwon and Kim, 2019; Kang et al., 2020).

The GEOPSY open-source software package (Geopsy Group, 2019; Wathelet et al., 2020) was used for single-station microtremor HVSR analyses. We followed and referenced the guidelines provided by Assatourians and Atkinson (2010) and Hassani and Atkinson (2016) to optimize parameters used in the GEOPSY analysis for calibration, windowing, tapering, and digital filtering. We applied a 5% cosine taper at the beginning and end of the microtremor records, and set the length of the signal processing time window for Fourier transform operation to 25.0 s. The parameter of the anti-triggering on signals was also applied to use only microtremor data except for seismic signals. A 0.1–50.0 Hz Butterworth filter was applied to the data and the Konno-Ohmach algorithm (Konno and Ohmachi, 1998) was used to smooth the horizontal and vertical Fourier amplitude spectra. The two horizontal-component amplitude spectra were calculated using a root-mean-square approach before the calculation of the HVSR.

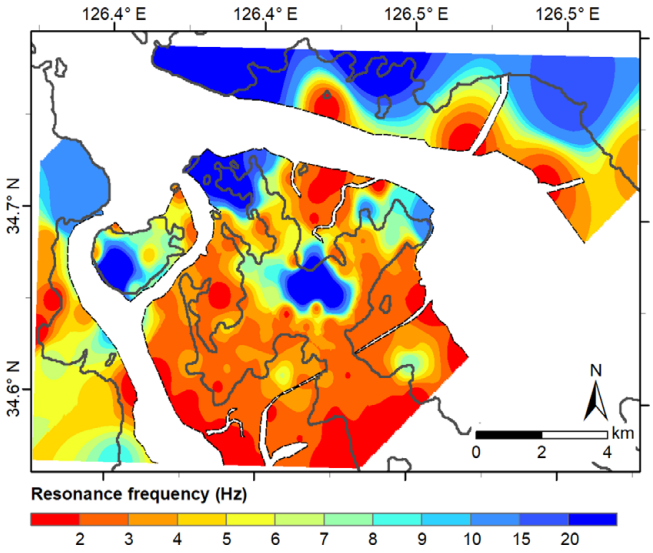

Fig. 6. Distribution of resonance frequencies across the study area from HVSR analysis. Solid lines represent the shoreline prior to the start of the large-scale land reclamation project in the late 1980s. The white space indicates areas of water where there was no site coverage (This version of figure with noise measurement locations is available in Fig. S1).

4. RESULTS

We recorded ambient noise at 144 sites throughout the study area and applied the single-station HVSR method to estimate the resonance frequencies at each site. We experienced difficulties identifying the fundamental resonance frequency for 12 sites, which have been excluded from the results. This may have been due to the presence of very stiff man-made materials (e.g., piled gravels) in shallow deposits from the ongoing land reclamation project, which could result in a weak impedance contrast with the basement. Excluding these 12 sites, we were able to successfully determine the fundamental resonance frequencies at 132 sites.

4.1. Resonance Frequency

Following Chatelain et al. (2008), we classify the 132 ambient noise sites into four groups based on their fundamental resonance frequencies (F_r) from HVSR analysis: low frequency sites satisfy the condition $F_r < 1$ Hz; medium frequency sites are defined by $1 \leq F_r < 5$ Hz; and high frequency sites satisfy $F_r \geq 5$ Hz. Ambient noise sites without any identifiable HVSR peaks are classified as "no peak" sites. Applying these criteria, the 132 sites are grouped into 102 medium frequency sites (77.3%), 22 high frequency sites (16.7%), and 8 "no peak" sites (6.0%). We did not identify any low frequency sites. Medium frequency sites are widely distributed throughout the study area except in the far north and a few scattered central part (Figs. 6 and S1 (electronic supplementary material)).

Typical examples of HVSR curves for medium and high frequency groups are found in Figures 5a and c, respectively. Figure 5b shows a HVSR curve with two apparent peaks, indicative of a site stratigraphy described by two layers over a basement. We interpreted the lower frequency (2.33 Hz) but smaller amplitude peak as the resonance frequency in this case. The HVSR curve shown in Figure 5a is associated with a site located near reclaimed land in the central part of the study area. Figure 5a shows only one peak at approximately 3.0 Hz in the HVSR curve and is a typical example of a medium-frequency site, located on a medium-thickness sedimentary layer overlying Jurassic granite bedrock (Fig. 3) (KIGAM, 2010). Figure 5c also shows an HVSR curve with a single peak (at 6.2 Hz) that is a typical example of a high-frequency site, located on a thin sedimentary layer with a basement of Cretaceous granite. The HVSR curve presented in Figure 5d

https://doi.org/10.1007/s12303-020-0040-9

is a typical example of a "no peak" site, with amplitudes of less than 2 across the frequency range considered in this study. No shallow sedimentary layers are expected to be present for "no peak" sites, and in the case of the site associated with Figure 5d the Cretaceous volcanic basement is exposed at the surface. In summary, lower fundamental resonance frequencies associated with thicker shallow deposits and low impedance are indicative of reclaimed land in the study area (Figs. 6 and S1), whereas higher resonance frequencies are expected at sites with a relatively thin sedimentary layer overlying Jurassic, Precambrian, or Cretaceous basement.

4.2. Depths to Bedrocks

The average shear-wave velocity of the shallow geology is estimated from MASW surveys at four sites within the study area. Three of the surveys are associated with medium frequency sites, while the other survey was completed at a high frequency site. Figure 7 shows the shear-wave velocity profiles at the four sites. At Station H007, which is located on Jurassic granite basement (Fig. 3a), the shear-wave velocity varies from 295 m/s to 392 m/s down to a depth of 9 m, below which it abruptly increases to 1204 m/s (Fig. 7a). Station H033 is located on the Jurassic formation (but adjacent to the reclaimed land). At this site, soft sediments with shear-wave velocities ranging from 195 m/s to 393 m/s appear to exist across the entire depth range of the MASW (i.e., 0–21 m) (Fig. 7b). Station H065 is located on reclaimed land. At this site, the shear-wave velocity ranges from 130 m/s to 173 m/s in the upper 7 m, and from 737 m/s to 893 m/s at depths of 7–30 m (Fig. 7c). Station H110 is located on a site where Cretaceous volcanic rocks are exposed at the surface. The shear-wave velocity at this site ranges from 1723 m/s to 1816 m/s between 0–19 m. From these MASW results, we find rocks in the Jurassic formation to have a mean shear-wave velocity of ~1200 m/s. Meanwhile, the rocks below the reclaimed land have a mean shear-wave velocity of ~810 m/s, which is significantly slower than that of the Jurassic rocks. The shear-wave velocity of the volcanic basement is ~1770 m/s, which is significantly faster than that of other rocks in the area.

We take 237 m/s as the average shear-wave velocity for shallow sediments, calculated from shear-wave velocities from H007, H033 and H065. For hard rock sites, where basement rocks are exposed at the surface, or where the fundamental resonance frequency is greater than 20 Hz, we used a mean shear-wave velocity of 1725 m/s as obtained from H110. Depths to the major impedance contrasts are then calculated using the resonance frequency and average shear-wave velocities (Eq. 1). They vary from 3 m to 56 m as shown in Figure 8 (also see Fig. S2 (electronic supplementary material)). As inferred from the distribution of resonance frequencies, areas of reclaimed land exhibit relatively thick unconsolidated material characterized by a low impedance. Comparing the estimates of sediment thicknesses from both MASW and HVSR techniques yields relatively consistent results.

4.3. Seismic Vulnerability of Ground Index (K_g)

We used peak resonance frequencies and amplifications of the horizontal to vertical motion to calculate the seismic vulnerability of

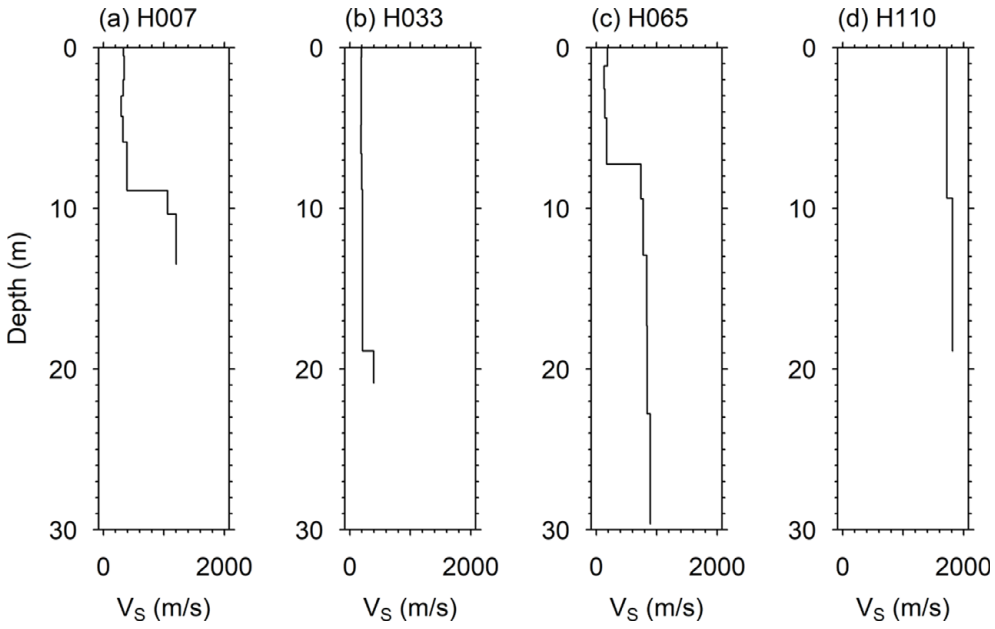

Fig. 7. Shear-wave velocity profiles obtained from the MASW at the four temporary stations. (a) H007, (b) H033, (c) H065, (d) H110.

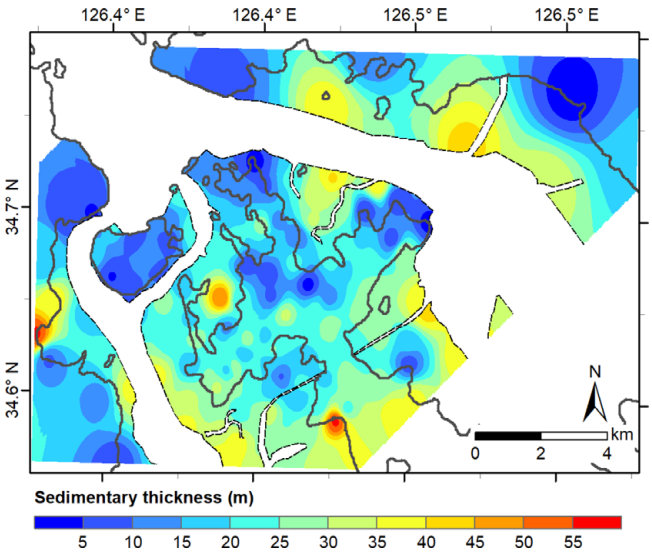

Fig. 8. Distribution of depths to bedrock across the study area, calculated from HVSR-derived resonance frequencies and MASW shear-wave velocities (This version of figure with noise measurement locations is available in Fig. S2).

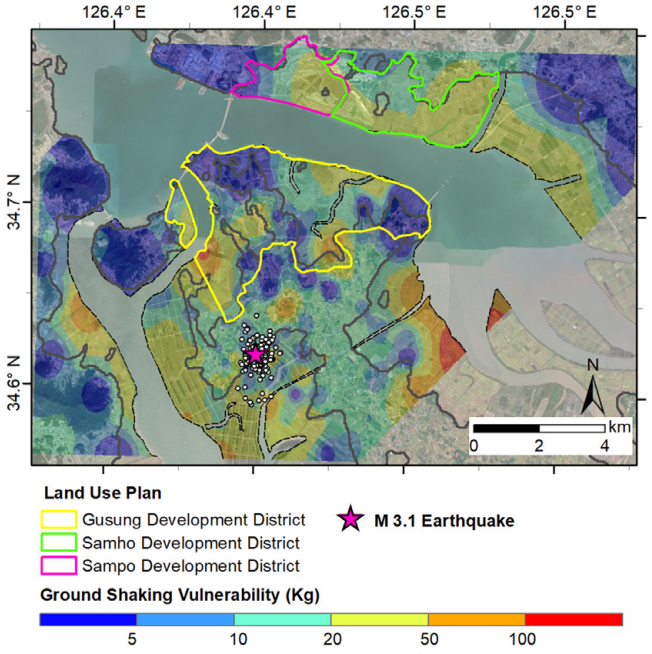

Fig. 9. Ground shaking vulnerability (based on the distribution of the seismic vulnerability index (M_g)) in the study area overlain by a land use plan for the SolaSeaDo urban development. Also shown are the epicentral locations of events from the 2020 Haenam earthquake swarm (white circles). The location of the highest magnitude event in the sequence is displayed as a purple star.

ground index (K_g) at each site (Fig. 9). Hardrock sites generally exhibit low K_g values, while K_g values are high (> 50) at sites situated on reclaimed land. We note that these indexes should be used with caution to distinguish relatively vulnerable zones.

5. DISCUSSIONS AND CONCLUSIONS

Seismic activity in the Haenam region of Korea has been very low since 1978, when modern seismic observations began in the country. A swarm of microearthquake activity began in the area on 26 April 2020 and lasted for approximately two weeks. During this period, the Korea Meteorological Administration reported 74 earthquakes in the region, including one that was widely felt by residents and caused serious concern to local and central authorities. The time-magnitude distribution of the earthquake sequence is indicative of swarm-type seismicity that lacks an identifiable mainshock, in contrast to the mainshock-aftershock or foreshock-mainshock-aftershock sequences more frequently observed in the Korean Peninsula.

Although the 2020 Haenam earthquake sequence was not destructive, the swarm-type earthquakes provide the motivation to assess the potential seismic hazard risks to the area. We studied the effects of one of the most well-observed earthquake swarms recorded since seismic monitoring began in Korea, and characterized the wider earthquake swarm area by presenting resonance frequencies, sediment thicknesses, and seismic vulnerability of ground indexes, estimated by HVSR. Relatively low resonance frequencies are estimated for areas of reclaimed land, which are interpreted to exhibit thicker, low impedance materials. We are reluctant to use the conventional term “sedimentary layer” to describe these materials, because it is clear that the area has been artificially filled since the late 1980s by materials related to the land reclamation project. In hard rock sites, higher resonance frequencies are estimated, which indicates shallower depths to major impedance contrasts associated with thin sedimentary layers.

K_g values are higher in areas of reclaimed land compared to hard rock sites. Since the K_g value is an intrinsic index that represents the vulnerability of the ground to earthquake shaking, areas with higher K_g indicate seismically vulnerable zones that may be prone to earthquake damage and require careful consideration during urbanization projects. It has been reported that areas of severe damage in the Marina District (a seaside neighborhood) of San Francisco, USA, caused by the 1989 M_w 6.9 Loma Prieta earthquake correspond to reclaimed land with $K_g > 20$. Much of the shallow geology across the Marina District consists of landfill, placed since 1869, associated with efforts to reclaim marshland and to infill a small baylet. The fill mostly comprises fine and silty sands, which were blamed for the widespread liquefaction (and related damage) experienced by the area in response to the earthquake (Holzer and O’Rourke, 1990; Seed et al., 1991). During the same earthquake, hillside areas characterized by $K_g < 20$ experienced only minimal damage (Nakamura, 1997; Liu et al., 2014). It is also reported that localized areas of large-

https://doi.org/10.1007/s12303-020-0040-9

scale liquefaction were associated with areas of higher K_g (> 10) during the 1999 M_w 7.7 Chi-Chi earthquake in Taiwan (Huang and Tseng, 2002). We note that although the interpretation of K_g is relatively intuitive – the higher the K_g value, the greater the influence of site effects, and so the greater the seismic hazard risk – it should be used with caution to assess seismic hazard risk, and an understanding of its limitations is critical in successful application of this index.

Local minima in the fundamental frequency distribution map (Fig. 6) indicate localized areas of thicker sediments or low-impedance materials. After a careful comparison with old satellite images, we attribute these areas to the deltas of ancient river mouths (Fig. 4a), which have been covered by material from land reclamation and so are not visible in the latest aerial photographs (Fig. 4b). We also observe that local areas of higher resonance frequencies correspond to areas where basement rocks are exposed at the surface. Improving the resolution of the distribution of fundamental frequencies is challenging and would require denser spatial coverage within the study area and a longer ambient noise observation period. As shear-wave velocity is expected to increase with depth, applying a mean shear-wave velocity to subsurface layers may result in under- or over-estimation of bedrock depth. Applying an empirical relationship between resonance frequency (obtained from HVSR analyses) and bedrock depth (obtained from boreholes) provides a better approximation.

The epicentral area of the 2020 Haenam earthquake swarm has experienced major changes associated with recent large-scale land reclamation (beginning in the late 1980s) and urban development (beginning in 2004). The new town districts (outlined in Fig. 9 on top of the K_g distribution map) are very close to the locations of the 2020 Haenam earthquake sequence and K_g values vary significantly across the study area. Larger K_g values may denote areas of increased seismic vulnerability and should be considered alongside HSVR resonance frequency data, amplification factors, and the thickness of low impedance materials or sediments to assess the risk posed to the urban development by earthquake ground motions.

ACKNOWLEDGMENTS

We would like to thank two anonymous reviewers for their critical review and comments. The author would also like to thank Hwanwoo Seo and Dr. Sinhang Kang for the MASW data acquisition. This study was supported by the Korean Meteorological Administration Research Development Program (grant no. KMI2018-02810) and the Basic Science Research Program through the National Research Foundation of Korea (NRF) funded by the Ministry of Education (NRF-2020R1I1A1A01053989).

REFERENCES

Abd El-Aal, A.E.A.K., 2010, Modelling of seismic hazard at the north-eastern part of greater Cairo metropolitan area, Egypt. Journal of Geophysics and Engineering, 7, 75–90.

Anderson, J.G., Bodin, P., Brune, J.N., Prince, J., Singh, S.K., Quaas, R., and Onate, M., 1986, Strong ground motion from the Michoacan, Mexico, Earthquake. Science, 233, 1043–1049. https://doi.org/10.1126/science.233.4768.1043

Assatourians, K. and Atkinson, G., 2010, Database of processed time series and response spectra data for Canada: an example application to study of 2005 M_N 5.4 Rivier du Loup, Quebec, Earthquake. Seismological Research Letters, 81, 1013–1031.

Becken, M., Ritter, O., Bedrosian, P.A., and Weckmann, U., 2011, Correlation between deep fluids, tremor and creep along the central San Andreas fault. Nature, 480, 87–90.

Bottelin, P., Dufréchou, G., Seoane, L., Llubes, M., and Monod, B., 2019, Geophysical methods for mapping Quaternary sediment thickness: application to the Saint-Lary basin (French Pyrenees). Comptes Rendus Geoscience, 351, 407–419.

Chang, S.-J. and Baag, C.-E., 2007, Moho depth and crustal Vp/Vs variation in southern Korea from teleseismic receiver functions: implication for tectonic affinity between the Korean Peninsula and China. Bulletin of the Seismological Society of America, 97, 1621–1631.

Chatelain, J.-L., Guillier, B., Cara, F., Duval, A.-M., Atakan, K., Bard, P.-Y., and The WP02 SESAME team, 2008, Evaluation of the influence of experimental conditions on H/V results from ambient noise recordings. Bulletin of Earthquake Engineering, 6, 33–74.

Chough, S.K., Kwon, S.-T., Ree, J.-H., and Choi, D.K., 2000, Tectonic and sedimentary evolution of the Korean peninsula: a review and new view. Earth-Science Reviews, 52, 175–235.

Dahm, T., Hrubcová, P., Fischer, T., Horálek, J., Korn, M., Buske, S., and Wagner, D., 2013, Eger Rift ICDP: an observatory for study of non-volcanic, mid-crustal earthquake swarms and accompanying phenomena. Scientific Drilling, 16, 93–99.

Geopsy Group, 2019, Geopsy Package Release 3.2.0. http://www.geopsy.org/download.php?platform=win64&release=3.2.0 [Accessed on 4 March 2019].

Google Earth, 2020, Images of Haenam, Korea, available on Google Earth between 1984 and 2020. http://www.google.com/earth/index.html [Accessed on 21 July 2020].

Han, J., Seo, W., Kim, H.-J., Kim, W.-Y., Won, D., Chung, J.-I., and Kim, K.-H., 2021, Monitoring a short-lived earthquake swarm during April–May 2020 in Haeman, Korea, and its preliminary results. Geosciences Journal, 25, 43–57.

Hardesty, K., Wolf, L.W., and Bodin, P., 2010, Noise to signal: a microtremor study at liquefaction sites in the New Madrid Seismic Zone. Geophysics, 75, B83–B90.

Hassani, B. and Atkinson, G.M., 2016, Applicability of the site fundamental frequency as a VS30 proxy for central and eastern North America. Bulletin of the Seismological Society of America, 106, 653–664.

Holzer, T.L., 1995, The Hanshin-Awaji (Kobe), Japan, Earthquake. GSA Today, 5, 154–167.

Holzer, T.L. and O'Rourke, T.D., 1990, Effects of the Loma Prieta earthquake on the Marina District, San Francisco, California. Open File Report No. 90-253, U.S. Geological Survey, Menlo Park, 128 p.

Hong, J.K., Kim, K.Y., and Choi, D.-L., 1999, A high-resolution seismic survey on the abandoned tidal flat in Shihwa Lake. Journal of the Korean Geophysical Society, 2, 251–258.

Huang, H.-C. and Tseng, Y.-S., 2002, Characteristics of soil liquefaction using H/V of microtremors in Yuan-Lin area. Taiwan Terrestrial, Atmospheric and Oceanic Sciences, 13, 325–338.

Ibs-von Seht, M. and Wohlenberg, J., 1999, Microtremor measurements used to map thickness of soft sediments. Bulletin of the Seismological Society of America, 89, 250–259.

Ishihara, K. and Koga, Y., 1981, Case Studies of Liquefaction in the 1964 Niigata Earthquake. Soils and Foundations, 21, 35–52.

Jeollanamdo, 2020, SolaSeaDo, Jeollanamdo Enterprise Cities Office. http://solaseado.go.kr/ [Accessed on 18 July, 2020]

Jou, H.-T., Kim, H.-J., Lee, G.-H., Lee, S.-H., Jung, B.-H., Cho, H.-M., and Jang, N.-D., 2008, Seismic imaging of a tidal flat: a case study for the Mineopo area. Mulli-Tamsa, 11, 197–203.

Kang, S.Y., Kim, K.-H., Chiu, J.-M., and Liu, L., 2020, Microtremor HVSR analysis of heterogeneous shallow sedimentary structures at Pohang, South Korea. Journal of Geophysics and Engineering. https://doi.org/10.1093/jge/gxaa035

KIGAM, 2010, Geology map of Korea, Korea Institute of Geosciences and Mineral Resources, Daejeon.

KIGAM, 2020, Geological Map of Korea, https://mgeo.kigam.re.kr/ [Accessed on March 10 2020].

Konno, K. and Ohmachi, T., 1998, Ground-motion characteristics estimated from spectral ratio between horizontal and vertical components of ambient noise. Bulletin of the Seismological Society of America, 88, 228–241.

Kwon, J. and Kim, K.-H., 2019, Ambient noise of temporary seismic stations in Gyeongju, Korea. The 74th Annual Meeting of the Geological Society of Korea and 2019 Fall Joint Conference of the Geological Sciences, Jeju, Oct. 23–26, p. 243.

Kyung, J.-B., 2021, Historical earthquake swarm (1565–1566) in the Sangwon area, Korea. Geosciences Journal, 25, 3–8.

Lachet, C. and Bard, P.-Y., 1994, Numerical and theoretical investigations on the possibilities and limitations of Nakamura's Technique. Journal of Physics of the Earth, 42, 377–397.

Lee, H., Kim, R., and Kang, T.-S., 2017, Seismic response from microtremor of Chogye Basin, Korea. Geophysics and Geophysical Exploration, 20, 88–95.

Lee, K. and Yang, W.-S., 2006, Historical seismicity of Korea. Bulletin of the Seismological Society of America, 96, 846–855. https://doi.org/10.1785/0120050050

Liu, L., Chen, Q.-F., Wang, W., and Rohrbach, E., 2014, Ambient noise as the new source for urban engineering seismology and earthquake engineering: a case study from Beijing metropolitan area. Earthquake Science, 27, 89–100.

Nakamura, Y., 1989, A method for dynamic characteristics estimation of subsurface using microtremor on the ground surface. Railway Technical Research Institute, Quarterly Reports, 30, 25–33.

Nakamura, Y., 1997, Seismic vulnerability indices for ground and structures using Microtremor. Proceedings of the World Congress on Railway Research (WCRR 97), Florence, Nov. 16–19, https://www.sdr.co.jp/papers/wcrr_vulnerability_indices.pdf [Accessed on January 5 2019].

Nakamura, Y., 2019, What is the Nakamura Method? Seismological Research Letters, 90, 1437–1443.

Park, C., 2018, ParkSEIS User Manual (Version 3.0). http://www.parkseismic.com/files/User_Manual_ParkSEIS_30_.pdf [Accessed on August 14 2020].

Park, C.B., Miller, R.D., and Xia, J., 1999, Multichannel analysis of surface waves. Geophysics, 64, 800–808.

Reiter, L., 1991, Earthquake Hazard Analysis: Issues and Insights. Columbia University Press, New York, 254 p.

Seed, R.B., Riemer, M.F., and Dickenson, S.E., 1991, Liquefaction of Soils in the 1989 Loma Prieta Earthquake. Proceedings of the 2nd International Converence on Recent Advances in Geotechnical Earthquake Engineering and Soil Dynamics, St. Louis, Mar. 11–15, p. 1575–1586.

Trunbull, M.L., 2009, Relative seismic shaking vulnerability microzonation using an adaptation of the Nakamura horizontal to vertical spectral ratio method. Journal of Earth System Science, 117, 879–895.

Wathelet, M., Chatelain, J.L., Cornou, C., Giulio, G.D., Guillier, B., Ohrnberger, M., and Savvaidis, A., 2020, Geopsy: a user-friendly open-source tool set for ambient vibration processing. Seismological Research Letters, 91, 1878–1889.

Xia, J., Miller, R.D., and Park, C.B., 1999, Estimation of near-surface shear-wave velocity by inversion of Rayleigh waves. Geophysics, 64, 691–700.

Yin, A. and Nie, S., 1993, An indentation model for the North and South China collision Tan-Lu and Honam fault systems, Eastern Asia. Tectonics, 12, 801–813.

https://doi.org/10.1007/s12303-020-0040-9